Icing Detection and Identification for Unmanned Aerial Vehicles: Multiple Model Adaptive Estimation

Andrea Cristofaro*, Tor Arne Johansen*, A. Pedro Aguiar†

***Abstract*— The accretion of ice layers on wings and control surfaces modifies the shape of the aircraft and, consequently, alters performance and controllability of the vehicle. In this paper we propose a multiple models adaptive estimation framework to detect icing affecting unmanned aerial vehicles using the following sensors: pitot tube (airspeed sensor), GPS, compass and IMU. A case-study is provided as support and validation of theoretical results.**

I. Introduction

Mechanical systems are usually exposed to possible malfunctions or anomalies; these may either be caused by faults occurring in actuators, effectors, sensors and other system components, or be structural, i.e. related to some modification of the nominal system dynamics. The problem of fault detection/identification and fault tolerant control has been widely investigated in recent years [1]; one of the major challenges to be faced in this topic is the correct identification of the fault behavior, in order to apply accommodation policies with the aim of recovering system performances or, at least, ensuring safe operational conditions.

Among structural faults, icing is a major issue for unmanned aerial vehicles (UAVs). The phenomenon of ice accretion on aircraft wings and control surfaces is a well recognized problem in aerospace engineering: when ice layers build up, they increase energy consumption and induce a safety risk, with the worst case scenario that the aircraft crashes [2] [3] [4]. Large airplanes are commonly equipped with efficient anti-icing and de-icing devices; however, these are unsuitable for small unmanned aircrafts, due to their simple architecture and limited payload. Ice formations on aerodynamic surfaces during flight are typically caused by the impact of supercooled water droplets (SWD). When a water droplet is cooled, it does not freeze until it reaches very low temperatures; however, the droplets will instantly freeze in the case of interaction with external agents, like aircrafts, releasing their own latent and accreting ice [5]. Both rate and amount of ice depend on the shape of the surface, its roughness, traveling speed, temperature and droplet size. Large SWD lead to the accretion of clear-ice, having a smooth and clear structure; it is usually characterized by horn-like formations on the wing leading edge [6] and it is the most dangerous type of icing. Rime ice, an opaque and rougher formation, is instead caused by the impact of small SWD. The modified shape of an aerodynamic surface due to ice changes lift, drag and pitch moment characteristics of the surface itself. For instance, an airfoil subject to horn-like ice formations may result in a lift coefficient reduction up to 40%, while the drag may be increased as much as 200%. A decrease in lift requires more engine power and implies a premature airfoil stall angle.

Very recently some advanced de-icing devices for UAV have been proposed based on carbon nanotubes technology [7] [8]; the wing surface can be painted with layers of coating material, which can be heated up very quickly using electricity. However, in order to guarantee the efficiency of the mechanism, it is very important to rely on icing detection and identification schemes with fast and accurate responses. Several approaches have been proposed for icing detection in aircrafts and unmanned aerial vehicles, namely actuator fault detection methods [9] [10] [11], Kalman filtering [12] or comparison methods for sensor failure diagnosis [13] [14]. In this paper we adopt a multiple-model (MM) approach [15] [16] [17] [18] [19] [20] [21]. Defining a bank of possible models, corresponding to distinct admissible values of the icing factor, the proposed algorithm guarantees the identification of the closest model to the true system as well as the estimation of the icing severity factor. The main advantages of the MM framework are cost-efficiency, robustness, parallel structure and fast transient response. The paper is structured as follows. The UAV model and the basic setup are given in Section II, while the MM framework is introduced in Section III. The main results are presented in Section IV. Finally, Section V is dedicated to the validation of the proposed results by means of numerical simulations.

II. UAV model

The longitudinal equations of rigid body motion of an aircraft are

$$\begin{cases} m(\dot{u} + qw - rv) = -mg\sin\theta - D\cos\alpha + L\sin\alpha + \mathcal{T} \\ \dot{q}I_{yy} - pr(I_{zz} - I_{xx}) + (p^2 - r^2)I_{xz} = M_A + M_{\mathcal{T}} \\ m(\dot{w} + pv - qu) = mg\cos\theta - D\sin\alpha - L\cos\alpha \end{cases}$$

where (u, v, w) are the velocities in the directions (x, y, z) w.r.t. the body-fixed frame, θ is the pitch angle, (p, q, r) are, respectively, the roll, pitch and yaw rates; I_{ij} are the coefficients of the inertia matrix, m is the mass of the aircraft, α is the angle of attack, D is the drag coefficient,

*A. Cristofaro and T.A. Johansen are with Department of Engineering Cybernetics, Norwegian University of Science and Technology and with Center for Autonomous Marine Operations and Systems (AMOS), Trondheim, Norway. email: andrea.cristofaro@itk.ntnu.no, tor.arne.johansen@itk.ntnu.no

†A.P. Aguiar is with the Department of Electrical and Computer Engineering, Faculty of Engineering, University of Porto (FEUP), Porto, Portugal. e-mail: pedro.aguiar@fe.up.pt.

A. Cristofaro acknowledges funding support from ERCIM Alain Bensoussan Fellowship programme (ABCDE project - FP7 Marie Curie Actions)

This work is part of the work carried out at AMOS. It is supported by the Research Council of Norway through the Centres of Excellence funding scheme, project No. 223254 - AMOS.

L is the lift coefficient, $\mathcal{T}$ is the thrust force and M_A, $M_{\mathcal{T}}$ are, respectively, the aerodynamical and thrust moments for the pitch. The above nonlinear model can be simplified by linearization with respect to some trim conditions; setting $c_\alpha := \cos\alpha_0$, the steady-state longitudinal linear dynamics is then given by [22]

$$\begin{bmatrix} \dot\nu \\ \dot\alpha \\ \dot q \\ \dot\theta \end{bmatrix} = \begin{bmatrix} X_\nu & X_\alpha c_\alpha & X_q & -g\cos\theta_0 \\ \frac{Z_\nu}{V_0 c_\alpha} & Z_\alpha & \frac{Z_q}{V_0 c_\alpha} & -\frac{g\sin\theta_0}{V_0 c_\alpha} \\ M_\nu & M_\alpha c_\alpha & M_q & 0 \\ 0 & 0 & 1 & 0 \end{bmatrix} \begin{bmatrix} \nu \\ \alpha \\ q \\ \theta \end{bmatrix} + \begin{bmatrix} X_{\delta_{th}} & X_{\delta_e} \\ 0 & \frac{Z_{\delta_e}}{V_0 c_\alpha} \\ M_{\delta_{th}} & M_{\delta_e} \\ 0 & 0 \end{bmatrix} \begin{bmatrix} \delta_{th} \\ \delta_e \end{bmatrix} = A_0 x + B_0 u. \tag{1}$$

The state variables x to be considered are the horizontal airspeed ν, the angle-of-attack α, the pitch rate q and the pitch angle θ. The symbols α_0, θ_0 and V_0 stand for some suitable trimmed values of angles and airspeed, respectively. The inputs $u = (\delta_{th}, \delta_e)$ entering the system are the engine throttle δ_{th} and the elevator deflection δ_e. The nominal parameters entering the system matrices can be expressed as follows

$$X_\ell = \mu_{X_\ell}\bar q C_{X_\ell},\ Z_\ell = \mu_{Z_\ell}\bar q C_{Z_\ell},\ M_\ell = \frac{\mu_{M_\ell}\bar q C_{M_\ell}}{I_{yy}}$$

with $\ell \in \{\nu, \alpha, q, \delta_{th}, \delta_e\}$ and where $\bar q = 1/2\rho V_0^2$ is the trimmed dynamic pressure (ρ being the air density) and the factors μ_i depend on the wing spanned area $\mathcal{S}$ and on the airfoil chord $\bar c$. The non-dimensional coefficients $C_{X_\ell}, C_{Z_\ell}, C_{M_\ell}$ are usually referred to as stability and control derivatives. The wind force can be modeled as an additive input vector given by

$$W_0 w = \begin{bmatrix} -\cos\theta_0 & -\sin\theta_0 \\ -\frac{\sin\theta_0}{V_0 c_\alpha} & \frac{\cos\theta_0}{V_0 c_\alpha} \\ 0 & 0 \\ 0 & 0 \end{bmatrix} \begin{bmatrix} w^{\mathrm{x}} \\ w^{\mathrm{z}} \end{bmatrix} \tag{2}$$

where w^{x} and w^{z} are the wind forces in the horizontal and vertical direction, respectively. Assuming that the UAV is equipped with an airspeed measurement device (pitot tube), compass, GPS and inertial sensors, all state variable are supposed to be available and hence the output matrix of the system is $C_0 = I_{4\times4}$; however, the measurements can be affected by noise and hence the output equation is given by

$$y(t) = x(t) + \omega(t),$$

where $\omega(t)$ is unknown but bounded.

A. Icing effect model

The accretion of clear ice on the aircraft surfaces modifies stability and control derivatives according to the following linear model [23]

$$C^\star_{\sharp_\ell} = (1 + \eta K_{\sharp_\ell}) C_{\sharp_\ell},\ \sharp = X, Z, M \tag{3}$$

with $\ell \in \{\nu, \alpha, q, \delta_{th}, \delta_e\}$ and where η is the icing severity factor and the coefficient K_i depends on aircraft specifications [4]; the clean condition corresponds to $\eta = 0$, while the all iced condition occurs for $\eta = \eta_{\max}$, where η_{max} can be determined by the peak in the drag force [3]. It is worth noticing that the coefficients K_i turn out to be negative, so that model (3) corresponds to downscaling of control and stabiliy derivatives.

As a consequence, the overall effect of icing can be modeled as an additive disturbance term $\mathcal{E}\eta$, where η is a scalar unknown quantity and the vector $\mathcal{E}$ is assigned by

$$\mathcal{E} = \begin{bmatrix} K_{X_\nu} X_\nu & K_{X_\alpha c_\alpha} X_\alpha & X_q & 0 \\ K_{Z_\nu}\frac{Z_\nu}{V_0 c_\alpha} & K_{Z_\alpha} Z_\alpha & K_{Z_q}\frac{Z_q}{V_0 c_\alpha} & 0 \\ K_{M_\nu} M_\nu & K_{M_\alpha} M_\alpha c_\alpha & K_{M_q} M_q & 0 \\ 0 & 0 & 0 & 0 \end{bmatrix} \begin{bmatrix} \nu \\ \alpha \\ q \\ \theta \end{bmatrix} + \begin{bmatrix} 0 & K_{X_{\delta_e}} X_{\delta_e} \\ 0 & K_{Z_{\delta_e}}\frac{Z_{\delta_e}}{V_0 c_\alpha} \\ 0 & K_{M_{\delta_e}} M_{\delta_e} \\ 0 & 0 \end{bmatrix} \begin{bmatrix} \delta_{th} \\ \delta_e \end{bmatrix} = A_K x + B_K u. \tag{4}$$

It is worth to note that icing may also alter the airspeed measurements, both directly and indirectly; in particular, ice formations inside the pitot tubes are not unlikely. Moreover, recalling that the angle of attack α is not directly measured but it is computed through airspeed [24], it follows that also its estimation may be subject to errors in the case of icing. We consider an additive model for the icing effect on the output, i.e. we suppose the output matrix to be given by $C_0 + \eta C_\sigma$, where

$$C_\sigma = [\sigma_\nu\ \sigma_\alpha\ 0\ 0]^T \tag{5}$$

is a known vector and η is the fault severity factor.

Remark 2.1: It can be noticed that the accretion of ice on airspeed sensors could be likely faster than on the aircraft surfaces, and that the effects are possibly more severe: this may result in the need of considering two distinct icing severity factors, namely body icing factor η^b and sensor icing factor η^s.

The following block diagram illustrates all possible interactions of icing with the UAV system.

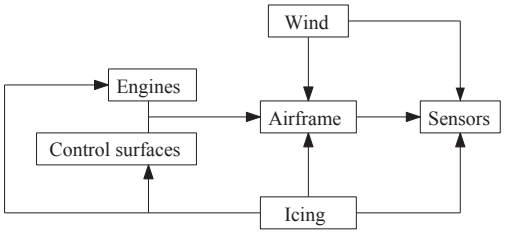

Fig. 1. Icing interaction with system components

III. A MULTIPLE-MODEL ADAPTIVE ESTIMATOR

Consider a LTI discrete-time plant of the form

$$\begin{aligned} x_{t+1} &= A_\kappa x_t + B_\kappa u_t + L_\kappa \xi_t \\ y_t &= C_\kappa x_t + \omega_t \end{aligned}$$

where $x_t \in \mathbb{R}^n$ denotes the state of the system, $u_t \in \mathbb{R}^m$ is the control input, $y_t \in \mathbb{R}^p$ is the output and $\xi_t \in \mathbb{R}^r, \omega_t \in \mathbb{R}^p$

are, respectively, bounded input and output noise terms. The system matrices $A_\kappa, B_\kappa, C_\kappa, L_\kappa$ contain unknown constant parameters denoted by the vector κ.

Consider a finite set of candidate parameter values $\mathbf{k} := \{\kappa_1, \kappa_2, ..., \kappa_N\}$; a multiple-model adaptive estimator (MMAE) can be designed according to

$$\hat{x}_t = \sum_{i=1}^{N} p_t^i \hat{x}_{t|\kappa_i} \tag{6}$$

$$\hat{y}_t = \sum_{i=1}^{N} p_t^i \hat{y}_{t|\kappa_i} \tag{7}$$

$$\hat{k}_t = k_{i^\star}, \quad i^\star := \arg \max_{i \in \{1,...,N\}} p_i^t \tag{8}$$

where $\hat{x}_t, \hat{y}_t$ and $\hat{k}_t$ are the estimates of the state, the output and the parameter vector at time t and p_t^i are dynamic weights to be defined. Each estimated state $\hat{x}_{t|\kappa_i}$ corresponds to the i^{th} Krener minimax observer [25]

$$\begin{aligned} \hat{x}_{t+1|\kappa_i} &= A_{\kappa_i}\hat{x}_{t|\kappa_i} + B_{\kappa_i}u_t + H_{\kappa_i}(y_t - C_{\kappa_i}\hat{x}_{t+|\kappa_i}) \\ \hat{y}_{t|\kappa_i} &= C_{\kappa_i}\hat{x}_{t|\kappa_i} \\ H_{\kappa_i} &= A_{\kappa_i}\Sigma_{\kappa_i}C_{\kappa_i}^T[C_{\kappa_i}\Sigma_{\kappa_i}C_{\kappa_i}^T + \Omega]^{-1}, \end{aligned}$$

with Σ_{κ_i} assigned by the discrete algebraic Riccati equation

$$\begin{gathered} -\Sigma_{\kappa_i} + A_{\kappa_i}^T\Sigma_{\kappa_i}A_{\kappa_i} + L_{\kappa_i}\Xi L_{\kappa_i}^T \\ -A_{\kappa_i}^T\Sigma_{\kappa_i}C_{\kappa_i}^T[C_{\kappa_i}\Sigma_{\kappa_i}C_{\kappa_i}^T + \Omega]^{-1}C_{\kappa_i}\Sigma_{\kappa_i}A_{\kappa_i} = 0, \end{gathered}$$

where Ξ and Ω are symmetric positive definite matrices, and the pairs $(A_{\kappa_i}, L_{\kappa_i})$ and $(A_{\kappa_i}, C_{\kappa_i})$ are controllable and observable, respectively.

The dynamic weights p_t^i are generated by the recursion

$$p_{t+1}^i = \frac{\beta_i e^{-\sigma_t^i}}{\sum_{j=1}^N p_t^j \beta_j e^{-\sigma_t^j}} p_t^i, \tag{9}$$

where β_i is a positive constant coefficient and σ_t^i is continuous function called error measuring function, mapping measurable plant signals to nonnegative values. These objects can be defined as follows:

$$\beta_i = \frac{1}{\sqrt{||S_{\kappa_i}||}}, \quad \sigma_t^i = \frac{1}{2}||y_t - \hat{y}_{t|\kappa_i}||_{S_{\kappa_i}^{-1}}$$

with $||x||_Q = (x^TQx)^{1/2}$ and where the positive definite matrix S_{κ_i} is given by

$$S_{\kappa_i} = C_{\kappa_i}\Sigma_{\kappa_i}C_{\kappa_i}^T + \Omega.$$

The dynamic weights are positive and they constitute a partition of unity. These properties are formally stated in the next theorem.

Theorem 3.1: Suppose that the initial conditions p_0^i satisfy $p_0^i \in (0,1)\ \forall i = 1, ..., N$ and $\sum_{i=1}^N p_0^i = 1$. Then each p_t^i is nonnegative, bounded and contained in the interval $[0,1]\ \forall t \geq 0$. Furthermore

$$\sum_{i=1}^{N} p_t^i = 1 \quad \forall t \geq 0.$$

Moreover, if a distinguishability condition is met, the dynamic weights satisfies an helpful convergence property.

Theorem 3.2: Let $i^\star \in \{1, 2, ..., N\}$ be an index of a parameter vector in $\mathbf{k}$ and set $\mathcal{I} := \{1, 2, ..., N\} \setminus i^\star$. Suppose that there exist positive constants n_1, t_1, ϵ and ϵ_1 such that for all $t \geq t_1$ and $n \geq n_1$ the following conditions hold:

$$\frac{1}{n}\sum_{\tau=t}^{t+n-1}(\sigma_\tau^{i\star} + \epsilon) < \frac{1}{n}\sum_{\tau=t}^{t+n-1}\min_{j\in\mathcal{I}}\sigma_\tau^j, \tag{10}$$

$$\log\max_{j\in\mathcal{I}}\beta_j - \log\beta_{i^\star} < \epsilon_1, \quad \textit{with } \epsilon_1 < \epsilon. \tag{11}$$

Then the dynamic weights p_t^i satisfy

$$\lim_{t\to\infty} p_t^{i^\star} = 1, \quad \lim_{t\to\infty} p_t^j = 0 \quad \forall j \in \mathcal{I}.$$

The proofs of Theorem 3.1 and Theorem 3.2 can be found in [18]. Let us stress that, although the theorem formulation is given in terms of a limit, the convergence rate of weights is typically very fast; moreover we point out that persistency of excitation may be a suitable condition to enhance distinguishability.

IV. Icing detection and identification

Let us consider the following discretized linear model derived from (1)-(2) by setting a sampling period $\tau_c > 0$ and assuming inputs and disturbances to be constant on each sampled interval:

$$\begin{aligned} x_{t+1} &= \bar{A}_0 x_t + \bar{B}_0 u_t + \bar{W}_0 w_t, \\ y_t &= \bar{C}_0 x_t + \omega_t \end{aligned}$$

where $\bar{A}_0 = e^{A_0\tau_c}$, $\bar{B}_0 = \int_0^{\tau_c} e^{A_0(\tau_c - s)}B_0 ds$, $\bar{W}_0 = \int_0^{\tau_c} e^{A_0(\tau_c-s)}W_0 ds$, $\bar{C}_0 = C_0$.

Assuming the icing severity factor to be slowly-variant, referring to (4), the icing conditions on the system can be expressed by the following matrices

$$\bar{A}_{ice}(\eta) = e^{(A_0 + \eta A_K)\tau_c}, \tag{12}$$

$$\bar{B}_{ice}(\eta) = \int_0^{\tau_c} e^{(A_0+\eta A_K)(\tau_c - s)}(B_0 + \eta B_K) ds, \tag{13}$$

$$\bar{W}_{ice}(\eta) = \int_0^{\tau_c} e^{(A_0+\eta A_K)(\tau_c-s)} W_0 ds, \tag{14}$$

$$\bar{C}_{ice}(\eta) = \bar{C}_0 + \eta C_\sigma \tag{15}$$

Let us assume the horizontal wind force w_t^{x} to be estimated through airspeed and GPS measurements, and for sake of clarity, set

$$\bar{W}_{ice}(\eta) = [\bar{X}_{ice}(\eta)\ \bar{Z}_{ice}(\eta)].$$

Select a set of parameter values $\mathcal{N} = \{\eta_1^0, ..., \eta_{N^*}^0\}$ with $\eta_i^0 < \eta_{i+1}^0$, $\eta_1^0 = 0$ and $\eta_{N^*}^0 \leq \eta_{max}$. In view of Remark 2.1, a vector

$$\eta_i = (\eta_i^b, \eta_i^s), \quad i = 1, ..., N \tag{16}$$

can be defined in order to consider different effects of icing on airfoils and sensors:

$$\begin{array}{llll} \eta_1 := (\eta_1^0, \eta_1^0) & \cdots & \eta_{N^*} := (\eta_{N^*}^0, \eta_1^0) \\ \eta_{N^*+1} := (\eta_1^0, \eta_2^0) & \cdots & \eta_{2N^*} := (\eta_{N^*}^0, \eta_2^0) \\ \vdots & \ddots & \vdots \\ \eta_{N-N^*} := (\eta_1^0, \eta_{N^*}^0) & \cdots & \eta_N := (\eta_{N^*}^0, \eta_{N^*}^0) \end{array}$$

where N can be easily computed as

$$N = N^* \cdot N^*.$$

Due to (12)-(15) and (16), one can define a bank of possible system models:

$$\mathcal{S}_i = \{A_{\eta_i}, B_{\eta_i}, C_{\eta_i}, X_{\eta_i}, Z_{\eta_i}\}, \quad i = 1, ..., N \tag{17}$$

with

$$\begin{array}{ll} A_{\eta_i} = \bar{A}_{ice}(\eta_i^b), & B_{\eta_i} = \bar{B}_{ice}(\eta_i^b), \\ X_{\eta_i} = \bar{X}_{ice}(\eta_i^b), & Z_{\eta_i} = \bar{Z}_{ice}(\eta_i^b) \\ C_{\eta_i} = \bar{C}_{ice}(\eta_i^s). & \end{array} \tag{18}$$

We point out that $\mathcal{S}_1$ corresponds to the nominal system, while $\mathcal{S}_N$ represents a model of the plant with total icing conditions.

Remark 4.1: The introduction of additional criterions to exclude the most unlikely events, allows us to reduce the number of models and the computational complexity.

In this way we can adopt the MMAE formulation and consider the family of minimax observers

$$\begin{aligned} \hat{x}_{t+1|\eta_i} &= A_{\eta_i}\hat{x}_{t|\eta_i} + B_{\eta_i}u_t + X_{\eta_i}w_t^{\mathrm{x}} + H_{\eta_i}(y_t - \hat{y}_{t|\eta_i}) \\ \hat{y}_{t|\eta_i} &= C_{\eta_i}\hat{x}_{t|\eta_i} \\ H_{\eta_i} &= A_{\eta_i}^T\Sigma_{\eta_i}C_{\eta_i}^T[C_{\eta_i}\Sigma_{\eta_i}C_{\eta_i}^T + \Omega]^{-1}, \end{aligned}$$

where the matrix Σ_{η_i} is the positive stabilizing solution of the discrete algebraic Riccati equation

$$\begin{gathered} -\Sigma_{\eta_i} + A_{\eta_i}^T\Sigma_{\eta_i}A_{\eta_i} + Z_{\eta_i}\Xi Z_{\eta_i}^T \\ -A_{\eta_i}^T\Sigma_{\eta_i}C_{\eta_i}^T[C_{\eta_i}\Sigma_{\eta_i}C_{\eta_i}^T + \Omega]^{-1}C_{\eta_i}\Sigma_{\eta_i}A_{\eta_i} = 0, \end{gathered}$$

with positive definite symmetric matrices Ω, Ξ to be computed based on the bounds on the output noise ω_t and on the vertical wind disturbance w_t^z, respectively. The overall estimated state $\hat{x}_t$, estimated output $\hat{y}_t$ and estimated icing factor $\hat{\eta}_t$ are obtained from the MMAE as the combinations (6)-(8), where the dynamic weights p_t^i are defined and updated according to (9).

Let us fix an arbitrary icing severity factor $\tilde{\eta} = (\tilde{\eta}^b, \tilde{\eta}^s) \in [0, \eta_{max}] \times [0, \eta_{max}]$, and consider the corresponding perturbed plant

$$\begin{aligned} x_{t+1} &= \bar{A}_{ice}(\tilde{\eta}^b)x_t + \bar{B}_{ice}(\tilde{\eta}^b)u_t + \bar{X}_{ice}(\tilde{\eta}^b)w_t^x + \bar{Z}_{ice}(\tilde{\eta}^b)w_t^z \\ y_t &= \bar{C}_{ice}(\tilde{\eta}^s)x_t \end{aligned} \tag{19}$$

Proposition 4.1: Let $\ell^b, \ell^s \in \{1, ..., N^* - 1\}$ be such that $\tilde{\eta}^b \in [\eta_{\ell^b}, \eta_{\ell^b+1}]$ and $\tilde{\eta}^s \in [\eta_{\ell^s}, \eta_{\ell^s+1}]$; assume in addition that the distinguishability conditions (10)-(11) are fulfilled. Then the overall estimated state $\hat{x}_t$ converges to the state $\hat{x}_{t|\eta_{\ell^*}}$ of the model $\mathcal{S}_{\ell^*}$ the closest to the true system x_t in the following sense:

$$p_t^{\ell^*} \to 1, \quad p_t^j \to 0 \ \forall j \neq \ell^* \tag{20}$$

where the index ℓ^* is characterized by the conditions

$$\begin{gathered} \textit{either } \eta_{\ell^*}^b = \eta_{\ell^b}^b \textit{ or } \eta_{\ell^*}^b = \eta_{\ell^b+1}^b \\ \textit{either } \eta_{\ell^*}^s = \eta_{\ell^s}^s \textit{ or } \eta_{\ell^*}^s = \eta_{\ell^s+1}^s. \end{gathered}$$

In particular, there exists $T_{\tilde{\eta}} > 0$ such that the pointwise set inclusions $\hat{\eta}_t^b \in \{\eta_{\ell^b}, \eta_{\ell^b+1}\}$, $\hat{\eta}_t^s \in \{\eta_{\ell^s}, \eta_{\ell^s+1}\}$ hold true for any $t \geq T_{\tilde{\eta}}$.

Proof: The statement follows straightforwardly from Theorem 3.2, provided that the list of claimed values $\mathcal{N}$ does not lead to indistinguishability scenarios. ■

Remark 4.2: We notice that, by construction, the procedure (18) yields distinct matrices for any different choice of parameters η^b, η^s, and therefore indistinguishability may only occur if the system output turns out to be equally distanced from two given models. However, for any fixed bank of MM, the largest set of icing values leading to such symmetry condition is a null-measure set.

Proposition 4.1 provides a method for extracting an estimation of the icing severity factor: the accuracy of the estimation depends on the number of multiple models being considered. However, the icing severity factor η is typically a time-variant quantity and therefore a method able to adapt to possible switches of η is desiderable. To this end, the update procedure (9) has to be modified in order to prevent the occurrence of the saturated scenario

$$p_t^h = 1, \ p_t^j = 0 \ \forall j \neq h \ \forall t > t_1.$$

Let us consider $\epsilon > 0$ sufficiently small, i.e. such that $\epsilon < 1/N$. For $\Delta > 0$, let us define the truncation operators

$$\begin{aligned} \mathrm{sat}_\Delta(s) &= \min(\Delta, \max(s, -\Delta)) \\ \mathrm{dead}_\Delta(s) &= s - \mathrm{sat}_\Delta(s) \end{aligned}$$

Define the weights p_i^t according to the following procedure:

$$\begin{cases} q_{t+1}^i = \frac{\beta_i e^{-\sigma_t^i}}{\sum_{j=1}^N p_t^j \beta_j e^{-\sigma_t^j}} p_t^i, \\ r_{t+1}^i = \sum_{j \neq i} \mathrm{dead}_{1-\epsilon}(q_{t+1}^j) \\ p_{t+1}^i = \mathrm{sat}_{1-\epsilon}(q_{t+1}^i) + \frac{r_{t+1}^i}{N-1} \end{cases} \tag{21}$$

Consider the following scenario, corresponding to a piecewise constant behavior of the icing factor:

- There exist two sequences of distinct values $\{\tilde{\eta}_1^b, ..., \tilde{\eta}_R^b\}$, $\{\tilde{\eta}_1^s, ..., \tilde{\eta}_R^s\}$ and a sequence of time instants $0 = t_0 < t_1 < \cdots < t_R$ such that
$$\tilde{\eta}^b \equiv \tilde{\eta}_j^b \text{ in } [t_{j-1}, t_j)$$
$$\tilde{\eta}^s \equiv \tilde{\eta}_j^s \text{ in } [t_{j-1}, t_j)$$
- The number N of assigned multiple models (17) is such that $N > R$ and moreover, for any $j = 1, ..., R$, there exist ℓ_j^b, ℓ_j^s with
$$\tilde{\eta}_j^b \in [\eta_{\ell_j}^b, \eta_{\ell_j^b+1}], \quad \tilde{\eta}_j^s \in [\eta_{\ell_j}^s, \eta_{\ell_j^s+1}].$$
- For any $k = 1, ..., R$ let $T_{\tilde{\eta}_k}$ be the estimation time horizon associated to the icing factor $\tilde{\eta}_k$, as defined in Proposition 4.1. Set
$$T_{\max} = \max_{k=1,...,R} T_{\tilde{\eta}_k} \tag{22}$$

Proposition 4.2: Assume that the length of time intervals $I_j = [t_{j-1}, t_j)$ is sufficiently large, i.e.

$$\min_{j=1,...,R} |I_j| > T_{\max}. \tag{23}$$

Then the modified weights (21) guarantee that the estimator $\hat{x}_t$ is able to adapt to the switching behavior of the parameter

$\tilde{\eta}$, *i.e. one has that for any* $j = 1, ..., R$ *there exists* $\tau_j \in I_j$ *with*

$$\hat{\eta}_t^b \in \{\eta_{\ell_j^b}, \eta_{\ell_j^b+1}\} \text{ for any } t \in [\tau_j, t_j),$$

$$\hat{\eta}_t^s \in \{\eta_{\ell_j^s}, \eta_{\ell_j^s+1}\} \text{ for any } t \in [\tau_j, t_j),$$

this corresponding to

$$\lim_{t \to t_j} p_t^{\ell_j^*} = 1 - \epsilon, \quad \lim_{t \to t_j} p_t^h = \epsilon/(N-1) \ \forall h \neq \ell_j^*$$

where, similarly to (20), ℓ_j^* *is assigned by*

$$\text{either } \eta_{\ell_j^*}^b = \eta_{\ell_j^b}^b \text{ or } \eta_{\ell_j^*}^b = \eta_{\ell_j^b+1}^b$$

$$\text{either } \eta_{\ell_j^*}^s = \eta_{\ell_j^s}^s \text{ or } \eta_{\ell_j^*}^s = \eta_{\ell_j^s+1}^s.$$

Proof: It sufficient to apply recursively the scheme given in Proposition 4.1: thanks to (22)-(23), the convergence is guaranteed on any subinterval I_j, $j = 1, ..., R$, with

$$\tau_j \leq t_{j-1} + T_{\max}.$$

Moreover, since the update algorithm (21) is introduced in order to prevent saturation, there is no need to re-initialize the weights p_t^j when switchings between subintervals I_j occur. ■

V. Simulations

Let us consider the case study of a typical small unmanned aircraft, the Aerosonde UAV (AAI Corporation, Textron Inc.). Initial conditions for the state variables have been chosen as follows: $\nu_0 = 22.9\ m/s$, $\alpha_0 = 0.1\ rad$, $q_0 = 0$, $\theta_0 = 0$. Assuming the air density $\rho = 1.2682\ Kg/m^3$, geometric and aerodynamical parameters of the aircraft are given in the following table [22]:

m	13.5 Kg		Z_ν	-0.5385 m/s^2
I_{xx}	0.8244 Kg/m^2		Z_α	-2.1277 s^{-1}
I_{yy}	1.135 Kg/m^2		Z_q	22.95 m/s
I_{zz}	1.759 Kg/m^2		M_ν	-0.1134 (m $\cdot$ s)$^{-1}$
I_{xz}	0.1204 Kg/m^2		M_α	-12.1204 s^{-2}
$\mathcal{S}$	0.55 m^2		M_q	-0.4602 s^{-1}
$\bar{c}$	0.1899 m		$X_{\delta_{th}}$	59.0570 s^{-1}
			X_{δ_e}	-0.4939 m/s^2
X_ν	-0.4365 s^{-1}		Z_{δ_e}	4.9230 m/s^2
X_α	-0.8802 m/s^2		$M_{\delta_{th}}$	0 (m $\cdot$ s)$^{-1}$
X_q	-2.3027 m/s		M_{δ_e}	-15.5248 s^{-2}

Using the coefficients listed above, the linearized longitudinal model (1) of the rigid-body aircraft system is derived. The aircraft attitude is supposed to be controlled by an autopilot, responsible to maintain the steady-state flight conditions in spite of wind disturbances. The wind speed components are assumed to be given by $w^x = 5.5m/s + noise$, $w^z = 0.5m/s + noise$. The simulated setup is the following:

- The measurements are supposed to be affected by a bounded noise term $\omega(t)$, with $||\omega(t)|| \leq 0.003$.
- The icing factor $\tilde{\eta} = (\tilde{\eta}^b, \tilde{\eta}^s)$ is supposed to be linearly increasing (see Fig. 2) and it is assigned by

$$\tilde{\eta}^b = \begin{cases} 0 & t \in [0, 25) \\ \text{linear} & t \in [25, 102) \\ 0.13 & t > 102 \end{cases}$$

$$\tilde{\eta}^s = \begin{cases} 0 & t \in [0, 9) \\ \text{linear} & t \in [9, 102) \\ 0.17 & t > 102 \end{cases}$$

- Assuming $\eta^b \leq \eta^s$ and restricting to the most likely scenarios only, seven multiple models have been considered, corresponding to the grid of four values $\eta_1^0 = 0, \eta_2^0 = 0.06, \eta_3^0 = 0.12$ and $\eta_4^0 = 0.18$:

$$\begin{array}{ll} \eta_1 = (0, 0), & \\ \eta_2 = (0, 0.06), & \eta_3 = (0.06, 0.06), \\ \eta_4 = (0.06, 0.12), & \eta_5 = (0.12, 0.12), \\ \eta_6 = (0.12, 0.18), & \eta_7 = (0.18, 0.18). \end{array}$$

The results are shown in Figs. 3-7: the norm of the true system output switches between the multiple-models as the icing severity factors increase, the weighted estimated output recovers the true system output and the correct estimation of the icing factors is achieved. The dynamic weights (21) have been implemented setting the saturation threshold $\epsilon = 0.02$. We notice that the proximity of two weights only occurs naturally during transients and hence distinguishability is guaranteed.

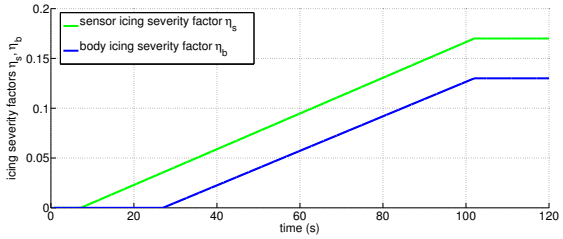

Fig. 2. Evolution of icing severity factor $\tilde{\eta}_t = (\tilde{\eta}_t^b, \tilde{\eta}_t^s)$

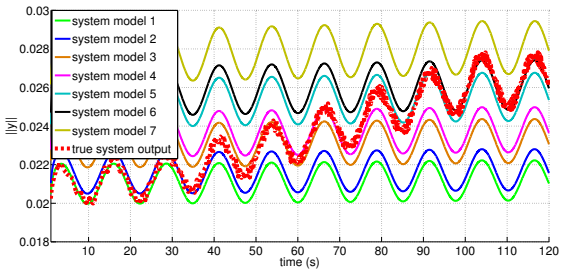

Fig. 3. Output norm: true system y_t vs MM $\hat{y}_{t|\eta_i}$, $i = 1, ..., 7$

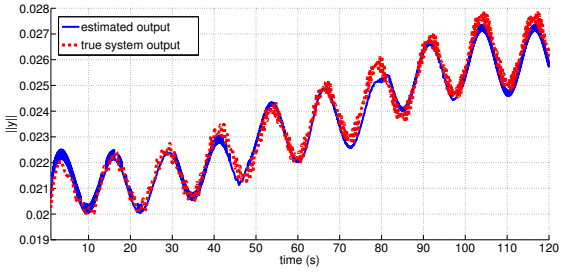

Fig. 4. Output norm: true system y_t vs weighted estimation $\hat{y}_t$

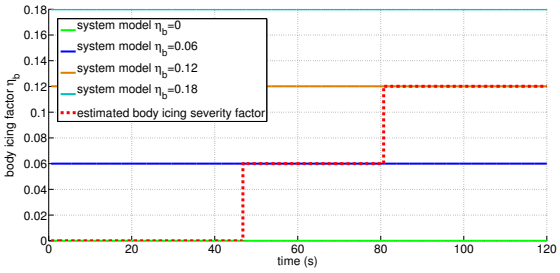

Fig. 5. Evolution of the estimated body icing factor $\hat{\eta}_t^b$

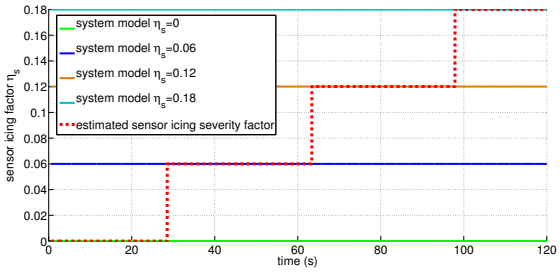

Fig. 6. Evolution of the estimated sensor icing factor $\hat{\eta}_t^s$

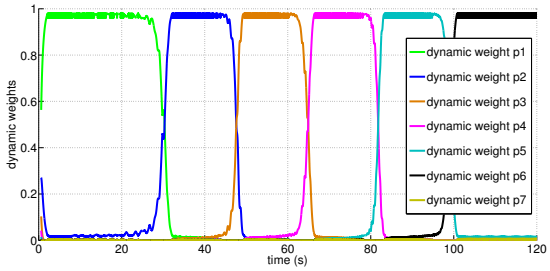

Fig. 7. Evolution of the dynamic weights $p_t^i,\ i = 1, ..., 7$

VI. Conclusions

In this paper the problem of icing detection and identification for small unmanned aerial vehicles is tackled using a multiple-model framework. Referring to the longitudinal model of the aircraft, which is assumed to be equipped with an airspeed sensor, a compass, a GPS and inertial sensors, a bank of possible system models is defined, each one corresponding to a different claimed value of the icing severity factor. Separate effects due to icing on the aerodynamic surfaces and on the airspeed sensors have been considered. The structure of the models is based on the classical Krener min-max observers, and overall state and icing factor estimates are obtained as weighted combinations of the states of the models and the claimed icing values, respectively. The proposed multiple-model estimator is shown to be able to cope with changes of the unknown parameters with a very fast transient response. Numerical simulations support and validate theoretical results: the MMAE-based icing detection and identification scheme has been applied to the case study of the Aerosonde UAV.

References

[1] Y. Zhang and J. Jiang, "Bibliographical review on reconfigurable fault tolerant control systems," *Ann. Rev. in Control*, vol. 32, pp. 229–252, 2008.

[2] R. W. Gent, N. P. Dart, and J. T. Cansdale, "Aircraft icing," *Phil. Trans. of the Royal Soc. of London. Series A: Mathematical, Physical and Engineering Sciences*, vol. 358, pp. 2873–2911, 2000.

[3] M. B. Bragg, T. Hutchison, J. Merret, R. Oltman, and D. Pokhariyal, "Effect of ice accretion on aircraft flight dynamics," *AIAA paper*, vol. 360, 2000.

[4] D. Pokhariyal, M. B. Bragg, T. Hutchison, and J. Merret, "Aircraft flight dynamics with simulated ice accretion," *AIAA Paper*, vol. 541, 2001.

[5] T. G. Myers and D. W. Hammond, "Ice and water film growth from incoming supercooled droplets," *Int. Journal of Heat and Mass Transfer*, vol. 42, pp. 2233–2242, 1999.

[6] M. B. Bragg, A. P. Broeren, and L. Blumenthal, "Iced-airfoil aerodynamics," *Progress in Aerospace Sciences*, pp. 323–362, 2005.

[7] S. Bone and M. Duff, "Carbon nanotubes to de-ice UAVs," *http://136.142.82.187/eng12/Author/data/2122.docx*, Technical report, 2012.

[8] K. L. Sørensen, A. S. Helland, and T. A. Johansen, "Carbon nanomaterial-based wing temperature control system for in-flight anti-icing and de-icing of unmanned aerial vehicles," *IEEE Aerospace Conference*, 2015.

[9] H. Miller and W. Ribbens, "Detection of the loss of elevator effectiveness due to aircraft icing," *37^{th} AIAA aerospace sciences meeting and exhibit, Reno*, 1999.

[10] M. Tousi and K. Khorasani, "Robust observer-based fault diagnosis for an unmanned aerial vehicle," in *Systems Conference (SysCon), 2011 IEEE International*, 2011, pp. 428–434.

[11] A. Cristofaro and T. A. Johansen, "An unknown input observer based approach for icing detection in unmanned aerial vehicles," *American Control Conference 2015*.

[12] F. Caliskan and C. Hajiyev, "A review of in-flight detection and identification of aircraft icing and reconfigurable control," *Progress in Aerospace Sciences*, vol. 60, pp. 12–34, 2013.

[13] S. Hansen and M. Blanke, "Diagnosis of airspeed measurement faults for unmanned aerial vehicles," *IEEE Transactions on Aerospace and Electronic Systems*, vol. 50, no. 1, pp. 224–239, 2014.

[14] G. Ducard, K. Rudin, S. Omari, and R. Siegwart, "Strategies for sensor-fault compensation on UAVs: Review, discussions and additions," in *13^th European Control Conference*, 2014, pp. 1963–1968.

[15] K. S. Narendra and J. Balakrishnan, "Adaptive control using multiple models," *Automatic Control, IEEE Transactions on*, vol. 42, no. 2, pp. 171–187, 1997.

[16] J. Kalkkuhl, T. A. Johansen, and J. Ludemann, "Improved transient performance of nonlinear adaptive backstepping using estimator resetting based on multiple models," *Automatic Control, IEEE Transactions on*, vol. 47, no. 1, pp. 136–140, 2002.

[17] J. Hansen and T. A. Johansen, "Transient performance, resetting and filtering in nonlinear multiple model adaptive control," in *American Control Conference*, 2004, pp. 1223–1228.

[18] V. Hassani, A. P. Aguiar, M. Athans, and A. M. Pascoal, "Multiple model adaptive estimation and model identification usign a minimum energy criterion," in *American Control Conference*, 2009, pp. 518–523.

[19] V. Hassani, A. Sorensen, A. M. Pascoal, and A. P. Aguiar, "Multiple model adaptive wave filtering for dynamic positioning of marine vessels," in *American Control Conference*, 2012, pp. 6222–6228.

[20] A. Hocine, M. Chadli, D. Maquin, and J. Ragot, "A discrete-time sliding window observer for markovian switching system," in *Proc. 45th IEEE Conf. on Decision and Control*, 2006, pp. 2661–2666.

[21] X.-R. Li and Y. Bar-Shalom, "Multiple-model estimation with variable structure," *Automatic Control, IEEE Transactions on*, vol. 41, no. 4, pp. 478–493, 1996.

[22] R. Beard and T. McLain, *Small unmanned aircrafts - Theory and practice*. Princeton University press, 2012.

[23] M. B. Bragg, T. Hutchinson, J. Merret, R. Oltman, and D. Pokhariyal, "Effect of ice accretion on aircraft flight dynamics," *Proc. 38th AIAA Aerospace Science Meeting and Exhibit*, 2000.

[24] J. Perry, A. Mohamed, B. Johnson, and R. Lind, "Estimating angle of attack and sideslip under high dynamics on small UAVs," in *ION GNSS Conference*, 2008, pp. 16–19.

[25] A. J. Krener, "Kalman-bucy and minimax filtering," *Automatic Control, IEEE Transactions on*, vol. 25, no. 2, pp. 291–292, 1980.